



## Quantum interference in strong-field ionization by a linearly polarized laser pulse and its relevance to tunnel exit time and momentum

Szabolcs Hack,<sup>1</sup> Szilárd Majorosi,<sup>2</sup> Mihály G. Benedict ,<sup>2</sup> Sándor Varró,<sup>1,3</sup> and Attila Czirják ,<sup>1,2,\*</sup>

<sup>1</sup>*ELI-ALPS, ELI-HU Non-Profit Ltd., W. Sandner str. 3, H-6728 Szeged, Hungary*

<sup>2</sup>*Department of Theoretical Physics, University of Szeged, Tisza L. krt. 84-86, H-6720 Szeged, Hungary*

<sup>3</sup>*Wigner Research Centre for Physics, Konkoly-Thege M. str. 29-33, H-1121 Budapest, Hungary*



(Received 24 March 2021; accepted 21 July 2021; published 9 September 2021)

We investigate the liberation of an atomic electron by a linearly polarized single-cycle near-infrared laser pulse having a peak intensity that ensures tunneling. Based on phase space analysis and energy distribution in the instantaneous potential, we reveal the importance of quantum interference between tunneling and over-the-barrier pathways of escape. Tunneling is blurred both in space and time, and the contribution of tunneling at the mean energy is almost negligible. We suggest and justify improved initial conditions for a classical particle approximation of strong-field ionization, based on the quantum momentum function, and we show how to reconstruct them from the detected momentum of an escaped electron.

DOI: [10.1103/PhysRevA.104.L031102](https://doi.org/10.1103/PhysRevA.104.L031102)

Strong-field ionization of atoms plays a fundamental role in attosecond physics [1,2]: a suitably strong laser pulse enables an electron to escape from its atomic bound state into the continuum, usually assumed to happen by tunneling, which is the first step of the very successful three-step model underlying much of our understanding in this area [3–7]. Currently, the problems of tunneling time and exit momentum are of outstanding importance regarding both quantum theory and attosecond metrology [8–12]. Several research groups published relevant experimental results [13–24], and some of these indicate a nonzero longitudinal exit momentum [13,16,18–21,24], either based on the attoclock method which relies on nearly circularly polarized pulses [14,16,25], or using linearly polarized pulses, sometimes along with weak auxiliary fields. For most of the established methods to generate attosecond pulses [26–30], laser pulse polarization is linear (at least in the middle of the pulse) and the Keldysh parameter  $\gamma$  [31] is close to 1, i.e., it is beyond the validity range of well-known theories [32]. Recent theoretical approximations of strong-field ionization meeting such conditions often employ classical dynamics, where the choice of proper initial conditions, including the longitudinal momentum, is an important open question [18,33–40], with controversies regarding, e.g., conservation of energy.

In this Letter, we reveal the real classical picture that can be associated with the exact quantum process of strong-field ionization of a single atom driven by a linearly polarized few-cycle laser pulse, in the  $\gamma \approx 1$  range. Our analysis using the Wigner function over the phase space inspires improved initial conditions for a set of classical electron trajectories which approximate the quantum evolution very well. Regarding model parameters, we focus on atomic hydrogen driven by a few-cycle pulse with a near-infrared carrier wavelength

and a peak intensity in the 100 TW/cm<sup>2</sup> range, which is a widespread case in theoretical works based on its relevance to state-of-the-art experimental techniques. We use atomic units unless otherwise stated.

We work in the framework of a simple model: we use dipole approximation for the interaction of a single active electron atom with the classical electromagnetic field in the length gauge. We define the laser pulse by the temporal pulse shape of its electric field along the  $z$  direction for  $0 < t < NT$  as  $\mathcal{E}_z(t) = F \sin^2(\pi t/NT) \cos(2\pi t/T + \phi)$ , having  $N$  optical cycles of period  $T$  and a carrier-envelope phase difference of  $\phi$ . This pulse excites the electron from its atomic ground state. The electron's wave function then does not depend on the azimuth angle around the  $z$  axis:  $\Psi = \Psi(z, \rho, t)$ , thus we can write the three-dimensional (3D) time-dependent Schrödinger equation (TDSE) for the electron's motion (assuming a fixed nucleus) in cylindrical coordinates  $(z, \rho)$  as

$$i \frac{\partial}{\partial t} \Psi = \left[ -\frac{1}{2} \left( \frac{\partial^2}{\partial z^2} + \frac{\partial^2}{\partial \rho^2} + \frac{1}{\rho} \frac{\partial}{\partial \rho} \right) + V(z, \rho, t) \right] \Psi, \quad (1)$$

with  $V(z, \rho, t) = -1/\sqrt{z^2 + \rho^2} + \mathcal{E}_z(t)z$ . Our recently developed algorithm [41] supports the direct numerical integration of this TDSE with Coulomb singularities and provides fourth-order accuracy in both space and time. In the following, the numerical results assume a laser pulse with  $N = 3$ ,  $T = 110$  (corresponding to  $\sim 800$  nm carrier wavelength) and  $\phi = 0$ , having an electric field amplitude of  $F = 0.06$  (corresponding to  $\sim 1.26 \times 10^{14}$  W/cm<sup>2</sup> peak intensity). These ensure that tunneling is possible during the entire laser pulse,  $\gamma = 0.952$ , and the pulse length is short enough to model high-order harmonic generation (HHG) resulting in an isolated attosecond pulse [26,27,42].

Since the main dynamics happens along the laser polarization [43], and a phase space analysis is more feasible in one dimension, we compute the one-dimensional (1D) reduced

\*czirjak@physx.u-szeged.hu

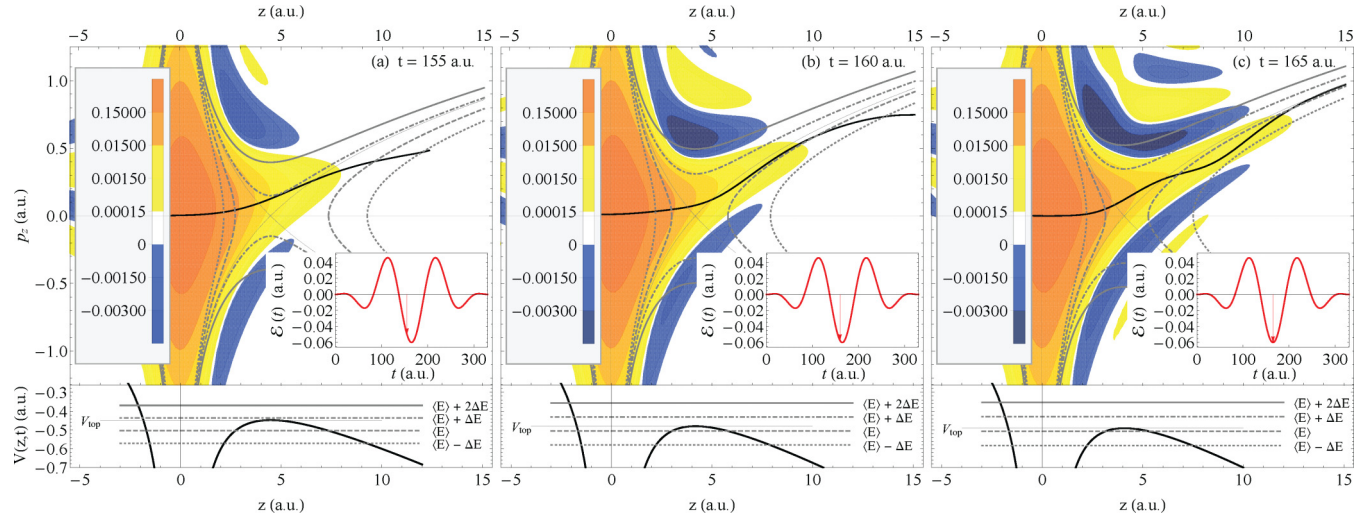


FIG. 1. Contour plots of the reduced 1D Wigner function of Eq. (3) in logarithmic color scheme (upper panels) and plots of  $V(z, 0, t)$  (lower panels, in black) at  $t = 155$  (a),  $t = 160$  (b), and  $t = 165$  (c) during the liberation of the hydrogen atom's electron by the laser pulse of the  $\mathcal{E}_z(t)$  plot in the insets. Phase space trajectories in gray with different styles represent classical motion in the instantaneous potential, corresponding to energy levels marked in the lower panels with respective styles. The trajectory with a thin gray solid line is the instantaneous separatrix between tunneling and OB ionization regimes. Black solid lines in the upper panels show the quantum momentum function of Eq. (4).

density matrix of the quantum state along the  $z$  axis from  $\Psi$  by integrating over the azimuth angle and radial coordinate:

$$\varrho(z, z', t) = 2\pi \int_0^\infty \Psi^*(z, \rho, t) \Psi(z', \rho, t) \rho d\rho. \quad (2)$$

Then we compute the corresponding Wigner function [44]

$$W(z, p_z, t) = \frac{1}{\pi} \int_{-\infty}^\infty \varrho(z + \zeta, z - \zeta, t) e^{2ip_z\zeta} d\zeta, \quad (3)$$

which is a successfully used tool also in strong-field and attosecond physics [45–50]. The main advantage of an analysis based on the Wigner function is that  $W$  displays the quantum description in a close analogy to the classical phase space dynamics, thus it enables one to use our intuition based on classical physics, while it still contains all the quantum details, most notably quantum interference [ $W$  is equivalent to  $\varrho$ , since Eq. (3) can be inverted].

Snapshots of this Wigner function at selected time instants close to and at the peak intensity of the laser pulse in Fig. 1 clearly show a developing stream in yellow (or in lightest gray in printed grayscale) along classical phase space trajectories of escaping particles, which already suggests that the liberation of the electron is blurred in time. (See [51] for an animation of the Wigner function during the whole laser pulse.) The oscillating ripples, including regions with negative function values, refer to strong quantum interference, similarly to earlier results with a simpler model [45]. The Wigner function's contour lines well follow the stationary phase space trajectories of classical particles with relevant energies in the instantaneous potential  $V(z, \rho, t)$ , including over-the-barrier (OB) ionization paths. This feature suggests the analysis of the energy distribution of the momentary quantum state, which we performed numerically in the instantaneous eigenstate basis of  $V$ , since we think this more appropriate than to follow the population of the unperturbed atomic bound states

[52]. The instantaneous energy probability densities, shown in Fig. 2, are sharply peaked around energy values which are close to but lower than the mean energy  $\langle E \rangle(t)$ . These peaks get broader and lower, and the population of the energy range above the top of the potential barrier  $V_{\text{top}}(t)$  increases considerably, as the laser pulse approaches its peak. Thus, the energy variance  $\Delta E(t)$  increases as well.

In order to evaluate the importance of the tunneling and OB ionization pathways, we compare the 1D probability currents  $j_{\text{FT}}(z, t)$  and  $j_{\text{OB}}(z, t)$  of the respective full tunneling (FT) and OB wave packets, shown in Fig. 3(a), which we compute using the instantaneous energy eigenstate decomposition, by integrating over all of the corresponding energy range below and above  $V_{\text{top}}(t)$ , respectively. These curves suggest that the resulting coherently summed full OB pathway is at

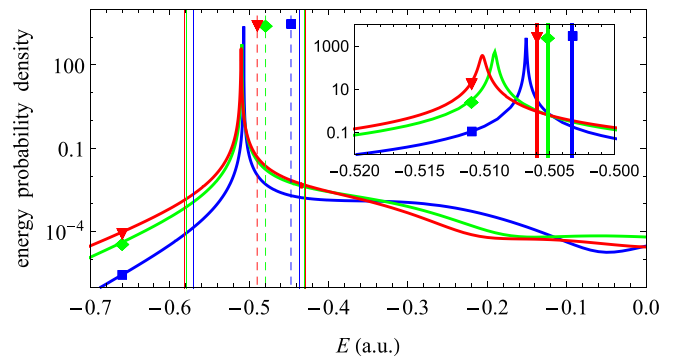


FIG. 2. Energy probability density of the quantum state at  $t = 155$  (blue,  $\blacksquare$ ),  $160$  (green,  $\blacklozenge$ ), and  $165$  (red,  $\blacktriangledown$ ) in the instantaneous potential. Thin solid vertical gridlines mark the  $\langle E \rangle(t) \pm \Delta E(t)$  values; dashed gridlines mark  $V_{\text{top}}(t)$ , with respective colors and symbols. The inset zooms in on the region around the peaks; thick solid gridlines mark  $\langle E \rangle(t)$ .

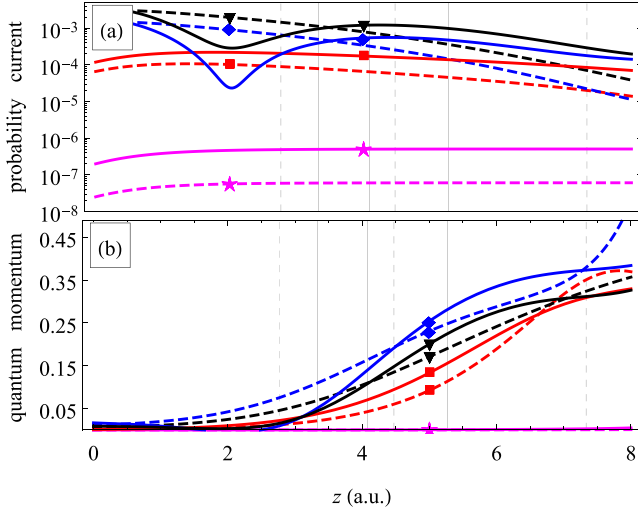


FIG. 3. Comparison of the probability currents  $j(z, t)$  (black,  $\blacktriangledown$ ),  $j_{\text{FT}}(z, t)$  (red,  $\blacksquare$ ),  $j_{\text{OB}}(z, t)$  (blue,  $\blacklozenge$ ), and  $j_{\text{ST}}(z, t)$  (magenta,  $\blackstar$ ) in (a), and the corresponding quantum momentum functions in (b). We plot these curves at the peak of the laser pulse  $t = 165$  (solid lines) and somewhat earlier at  $t = 155$  (dashed lines). The vertical gridlines mark the momentary positions of the tunnel entrance, the  $V_{\text{top}}(t)$ , and the tunnel exit, from left to right, with respective style.

least as important as the resulting coherently summed full tunneling pathway of ionization. Comparing them to the total probability current  $j(z, t)$  obviously shows strong interference between them. We would like to emphasize that this full tunneling pathway significantly expands the most widespread view of tunnel ionization, when tunneling is considered usually at the initial bound state energy or at the mean value of the energy. In order to highlight this difference, we also plot the probability current  $j_{\text{ST}}(z, t)$  of a such a sharp tunneling (ST) wave packet, which we create by integrating over a narrow energy range of 0.004 a.u. centered at the mean value of the energy. The  $j_{\text{ST}}(z, t)$  is two to three orders of magnitude smaller than the full tunneling current  $j_{\text{FT}}(z, t)$ , and this fact does not change qualitatively, if the narrow energy range is centered at the peak of the energy probability density. This seemingly surprising difference may be well explained by the “laser acceleration” beyond the tunnel exit for those components which tunneled out at higher energy levels. However, the above results actually question the justification of a sharply defined position and time instant for the tunnel exit.

Due to the essential role of quantum interference during the escape, the classical particle model of the escaping electron should account for all of the possible pathways. One of the most important open questions for such a classical particle is a properly chosen initial momentum. This is in close connection with the Wigner function, since its meaning leads intuitively to the notion of a position-dependent average momentum in terms of its  $n$ th moment  $P_n(z, t) = \int_{-\infty}^{\infty} p_z^n W(z, p_z, t) dp_z$  as

$$q(z, t) = P_1(z, t)/P_0(z, t), \quad (4)$$

which is in fact identical to the gradient of the Madelung phase (multiplied by  $\hbar$ ), usually called quantum momentum function or flow momentum [53]. We plot the quantum momentum function  $q(z, t)$  in the phase space snapshots of Fig. 1 with

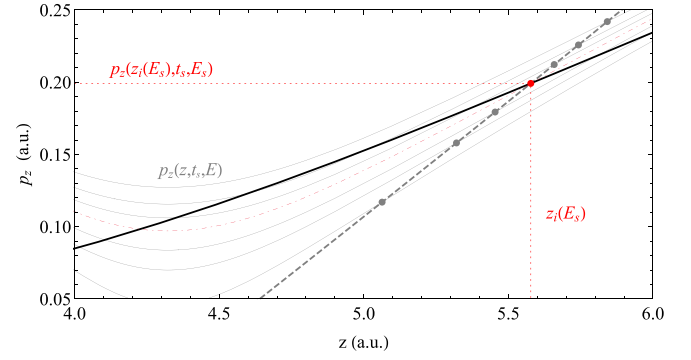


FIG. 4. Definition of the initial phase space point (shown for  $t_s = 157$ ): there is only a single inflection point (along the dot-dashed line in red) among the inflection points (dashed line and dots in gray) of the stationary phase space trajectories (gray solid lines) of the instantaneous potential, which is on the instantaneous quantum momentum function (black solid line).

a black solid line: it follows very well the main stream of the Wigner function corresponding to an escaping particle in the spatial domain where the electron’s probability density is significant. Its developing oscillations are due to quantum interference of the ionization pathways with different energies. Figure 3(b) shows clearly the interference between the quantum momenta of the FT and OB wave packets, and the negligible quantum momentum of the ST wave packet.

Next we show that properly chosen initial conditions enable a suitable set of classical trajectories that follow the quantum momentum function very well and they also reflect that the liberation process is blurred both in space and time. Based on its physical meaning, it is intuitive to use a suitable point of the quantum momentum function itself as the initial condition of a possible classical trajectory which starts at the instant  $t_s$  from the phase space point  $[z_s, q(z_s, t_s)]$ . This initial  $z_s$  coordinate should be chosen in such a way, that the quantum propagation of the escaping wave packet beyond  $z_s$  can be approximated by classical dynamics with sufficient accuracy, but it is still close enough to the position of the local maximum of the potential barrier so that it is relevant as the initial position of an escaping trajectory. A reasonable balance of the latter two requirements is provided by the position  $z_i(E)$  of the outermost inflection point of a suitable stationary phase space trajectory of the instantaneous potential, given by  $p_z(z, t_s; E) = \sqrt{2[E - V(z, 0, t_s)]}$  for total energy  $E$ . We plot these trajectories and the corresponding inflection points for a few of the continuum values of  $E$  in Fig. 4. The  $p_z(z, t_s; E)$  are concave for  $z > z_i(E)$ , because the dynamics is dominated by the laser electric field, which allows a classical approximation. Taking into account now all of the above considerations, it follows that the initial position  $z_s$  we seek is actually the position of that particular inflection point where the corresponding stationary phase space trajectory intersects the quantum momentum function (see the dot-dashed red curve and the solid black curve in Fig. 4). Denoting the corresponding energy by  $E_s$ , the  $z_i(E_s)$  selected by the quantum momentum function is the solution of the following equation:

$$q(z_i(E_s), t_s) = p_z(z_i(E_s), t_s; E_s). \quad (5)$$

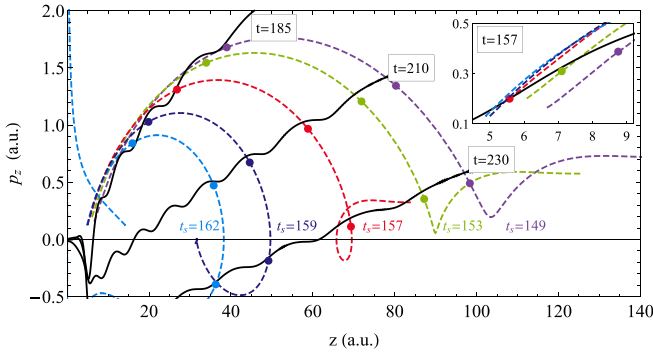


FIG. 5. Classical phase space trajectories of the liberated electron (dashed lines) for the indicated starting time instants, plot from  $t_s$  to  $t = NT$ . Initial conditions correspond to Eq. (5); the inset zooms in to the phase space region around these start points. Directly escaping trajectories are represented and marked by  $t_s = 149, 153,$  and  $157$  (in purple, green, and red, respectively). The  $t_s = 159$  (in dark blue) marks a limiting case having  $\sim 0$  momentum at  $t = NT$ . The  $t_s = 162$  (in light blue) marks a rescattering trajectory. Snapshots of the classical and the quantum propagation at  $t = 157, 185, 210,$  and  $230$ , represented by the dots and by  $q(z, t)$  (black solid line), respectively, show a good match for all of the different outcomes.

At every realistic starting time  $t_s$ , there is only a single solution  $z_i(E_s)$  of Eq. (5). We propose this as the initial position,  $z_s = z_i(E_s)$ , and the unique phase space point  $[z_s, q(z_s, t_s)]$  as the initial state of the classical escape trajectory which starts at  $t_s$ . This initial state is always in the OB regime but, as we shall see, it is still a good classical representation of all possible escape pathways depending on the starting time. We plot several phase space trajectories and some characteristic snapshots of the dynamics of the escaping electron for different starting time instants in Fig. 5. The electron is close to the quantum momentum function during the whole propagation, regardless of the starting time, which well justifies that they represent a good classical approximation of the true quantum dynamics. As the  $t_s$  values get closer to the instant of the main peak of the laser pulse, for  $t_s > 157$  the electron does not have enough kinetic energy at the end of the interaction to leave its parent ion permanently. For further increasing starting time instants, the electron is rescattered with energy gain from the laser pulse and it may thus contribute, e.g., to HHG. The starting positions are in good agreement with earlier data derived from experiments [8].

We can gain more insight into the onset of the escape process by studying a wave packet which is defined to have positive momentum and positive energy (PMPE) at the final instant of the laser pulse: i.e., we obtain this PMPE wave packet by first subtracting the contributions of the bound states  $|n, \ell\rangle$  from the 3D solution at  $t = NT$ :

$$|\Psi_{\text{PE}}(t = NT)\rangle = |\Psi(t = NT)\rangle - \sum_{n, \ell} \langle n, \ell | \Psi \rangle |n, \ell\rangle \quad (6)$$

and then keeping (by Fourier filtering) only those components of  $|\Psi_{\text{PE}}(t = NT)\rangle$  which have positive  $p_z$ . In an ideal case, this PMPE wave packet is able to reach a detector at a macroscopic distance (placed at a position with a large

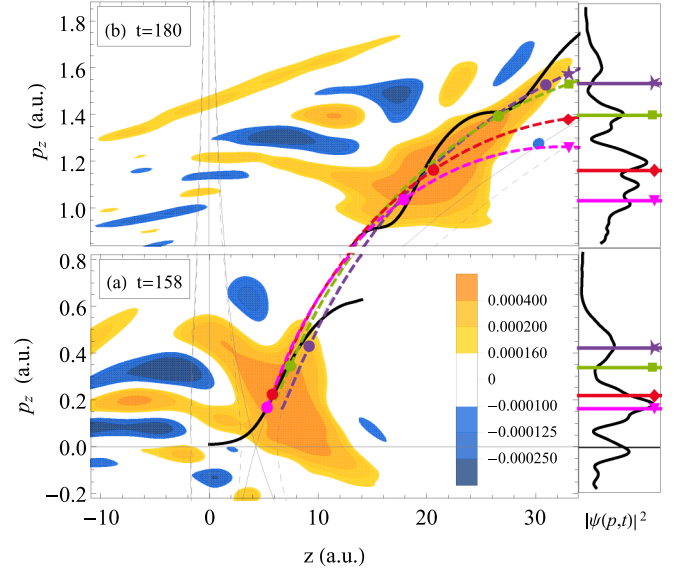


FIG. 6. Comparison of classical and PMPE quantum dynamics of an escaping electron at  $t = 158$  (a) and at  $t = 180$  (b). Left panels: colored contour plots of  $W_{\text{PMPE}}$  and plot of  $q(z, t)$  (solid black line). Solid and dashed thin gray trajectories are as in Fig. 1. Dashed lines in purple (marked by ★), green (■), red (◆), and magenta (▼) show classical trajectories starting at  $t_s = 149, 153, 157,$  and  $158$ , respectively, having different initial conditions according to Eq. (5). Dots on each of these dashed lines mark the momentary state of the classical dynamics. Right panels: momentum distribution of the PMPE wave packet (black solid line) and momentum values relevant to classical dynamics marked with gridlines in respective colors and symbols.

positive  $z$  coordinate). However, we now propagate this 3D PMPE wave packet backwards in time using the 3D TDSE (1) and then we do a phase space analysis of the resulting 1D Wigner function  $W_{\text{PMPE}}(z, p_z, t)$  which we obtain from the 3D PMPE wave packet just as we obtained  $W(z, p_z, t)$  from the full 3D wave function  $\Psi(z, \rho, t)$ . We compare the classical trajectories according to the initial conditions of Eq. (5) with the  $W_{\text{PMPE}}(z, p_z, t)$  in Fig. 6. The snapshot at  $t = 159$  clearly shows that besides tunneling, the OB pathway is essential also in the escape of the PMPE wave packet. If a single “privileged” classical trajectory should be chosen, the one starting at  $t = 157$  a.u. seems to be the good representation of this process. However, a suitable set of such trajectories with different starting times gives apparently a better approximation of the quantum dynamics of the PMPE wave packet, and such a set reflects also the temporally blurred feature of the liberation process. This approach is further supported by the observation that the Wigner function approximately follows the classical propagation during its time evolution, in agreement with the well-known fact that for potentials with up to quadratic spatial dependence (which is a good approximation in the relevant spatial domain of  $W_{\text{PMPE}}$ ) the quantum Liouville equation is identical to the classical one. This makes the assignment of probabilities to these trajectories possible and meaningful.

Finally, we show how a simple procedure can reconstruct the starting time from the detected momentum of a directly escaped electron. Neglecting the Coulomb interaction first, the

TABLE I. Comparison of real starting times ( $t_s$ ) and reconstructed starting times ( $t_s^R$ ) obtained from the method described in the main text.

$t_s$	149	151	153	154	155	156	157
$t_s^R$	151.88	153.11	153.99	154.47	155.06	155.84	156.84

momentum of the electron at the end of the laser pulse would be the following:

$$p_f^{\text{NC}} = p_0 + \int_{t_s}^{t_f} e\mathcal{E}_z(t) dt, \quad (7)$$

where  $p_0$  is unknown if  $t_s$  or  $q(z, t)$  is unknown. In reality, the escaping electron interacts with its parent ion's Coulomb potential until it reaches the detector at infinity where its measured momentum is  $p_d = \sqrt{(p_f^{\text{C}})^2 + 2V_f^{\text{C}}}$  in terms of its potential energy  $V_f^{\text{C}}$  and momentum  $p_f^{\text{C}}$  at  $t_f = NT$ . Denoting by  $\Delta W$  the difference of the work of the laser electric field on the trajectories with and without the Coulomb interaction, we get

$$p_f^{\text{NC}} = \sqrt{p_d^2 - 2(V_0^{\text{C}} + \Delta W)}, \quad (8)$$

where  $V_0^{\text{C}}$  is the potential energy of the electron in the Coulomb field at  $t_s$ . The energy in parentheses can be approximated well in terms of the initial coordinate  $z_0$  as  $V_0^{\text{C}} + \Delta W = -1/z_0$ . Equations (8) and (7), and Eq. (5) with  $q$  replaced by  $p_0$ , enable an iterative procedure to reconstruct the value of  $t_s$  from  $p_d$ , based on realistic starting values of  $p_0$  and  $z_0$ . In order to test the accuracy of this procedure, we generated the  $p_d$  values in a “numerical experiment”: we computed the final momenta of escaping classical trajectories according to the initial conditions of Eq. (5) for a set of  $t_s$  which are relevant for the PMPE wave packet. Then we applied the above iterative procedure to obtain the reconstructed values of the starting time:  $t_s^R$ . The results listed in Table I show that, although the largest error exceeds 2 a.u. for the earliest starting times, the accuracy greatly improves for more probable trajectories and the error may get even below 5 attoseconds for  $155 \leq t_s \leq 157$ . Note that the corresponding phase space trajectories follow the larger values of the PMPE Wigner function.

In conclusion, our results provide important and detailed insight into the process of atomic strong-field ionization by a linearly polarized single-cycle laser pulse. We investigated the Keldysh parameter range of  $\gamma \approx 1$ , which is typical in

many of the relevant experiments but it lacks exact analytic theory. Based on accurate numerical simulations, important features of the electron's motion are shown by the Wigner function intuitively: the escaping wave packets create streams and oscillating ripples as a manifestation of quantum interference, which also rotate clockwise around the central bound part as the laser electric field drives the process (see the animation [51]). Our primary purpose was to explore the quantum details of the electron's liberation around the main peak of the laser pulse. Interference between components tunneling with different energies [below  $V_{\text{top}}(t)$ ] makes both the time and the position of the tunnel exit blurred, which questions the usual picture of strong-field tunneling. Both the Wigner function and the probability currents show that the over-the-barrier pathways have an important contribution to the liberation, despite  $\langle E \rangle(t) < V_{\text{top}}(t)$ . These explain experimental results on nonzero longitudinal momentum at the tunnel exit, which apparently contradict energy conservation according to the definition of a sharp tunnel exit. We showed that the Wigner function naturally inspires one to use the quantum momentum function and that this enables new initial conditions [Eq. (5)] for classical approximation with nonzero initial longitudinal momentum. The resulting classical trajectories follow the quantum evolution very well; they account for direct escape and rescattering, depending on start time, and a suitable set of such trajectories reflects the blurred nature of the liberation process. The presented results were checked to be qualitatively valid for  $F = 0.04\text{--}0.06$  and  $\phi = 0, \pi/4, \pi/2, 3\pi/4$ . We believe that the Wigner function will be useful in further analysis of strong-field ionization, especially if quantum interference has an important role, like, e.g., in rescattering, above-threshold ionization, and low-energy structures.

We thank Wilhelm Becker, Péter Földi, Balázs Major, and Katalin Varjú for valuable discussions. This research was performed in the framework of the project No. GINOP-2.3.2-15-2016-00036, and also supported by the European Union, cofinanced by the European Social Fund, Grant No. EFOP-3.6.2-16-2017-00005. Partial support by the ELI-ALPS project is also acknowledged. The ELI-ALPS project (GINOP-2.3.6-15-2015-00001) is supported by the European Union and cofinanced by the European Regional Development Fund. This work was supported by the Ministry of Innovation and Technology, Hungary Grant No. NKFIH-1279-2/2020.

[1] F. Krausz and M. Ivanov, *Rev. Mod. Phys.* **81**, 163 (2009).  
 [2] G. Farkas and C. Tóth, *Phys. Lett. A* **168**, 447 (1992).  
 [3] P. B. Corkum, *Phys. Rev. Lett.* **71**, 1994 (1993).  
 [4] S. Varró and F. Ehlotzky, *Il Nuovo Cimento D* **15**, 1371 (1993).  
 [5] M. Lewenstein, P. Balcou, M. Y. Ivanov, A. L'Huillier, and P. B. Corkum, *Phys. Rev. A* **49**, 2117 (1994).  
 [6] W. Becker, S. Long, and J. K. McIver, *Phys. Rev. A* **50**, 1540 (1994).  
 [7] M. Y. Ivanov, M. Spanner, and O. Smirnova, *J. Modern Opt.* **52**, 165 (2005).

[8] D. D. Hickstein, P. Ranitovic, S. Witte, X. M. Tong, Y. Huis-mans, P. Arpin, X. Zhou, K. E. Keister, C. W. Hogle, B. Zhang *et al.*, *Phys. Rev. Lett.* **109**, 073004 (2012).  
 [9] L. Guo, S. S. Han, X. Liu, Y. Cheng, Z. Z. Xu, J. Fan, J. Chen, S. G. Chen, W. Becker, C. I. Blaga *et al.*, *Phys. Rev. Lett.* **110**, 013001 (2013).  
 [10] D. Guénot, D. Kroon, E. Balogh, E. W. Larsen, M. Kotur, M. Miranda, T. Fordell, P. Johnsson, J. Mauritsson, M. Gisselbrecht *et al.*, *J. Phys. B: At., Mol. Opt. Phys.* **47** (2014).  
 [11] A. S. Landsman and U. Keller, *Phys. Rep.* **547**, 1 (2015).

- [12] A. S. Kheifets, *J. Phys. B: At., Mol. Opt. Phys.* **53**, 072001 (2020).
- [13] D. Comtois, D. Zeidler, H. Pépin, J. C. Kieffer, D. M. Villeneuve, and P. B. Corkum, *J. Phys. B: At., Mol. Opt. Phys.* **38**, 1923 (2005).
- [14] P. Eckle, A. N. Pfeiffer, C. Cirelli, A. Staudte, R. Dörner, H. G. Muller, M. Büttiker, and U. Keller, *Science* **322**, 1525 (2008).
- [15] M. Schultze, M. Fieß, N. Karpowicz, J. Gagnon, M. Korbman, M. Hofstetter, S. Neppl, A. L. Cavalieri, Y. Komninos, Th. Mercouris *et al.*, *Science* **328**, 1658 (2010).
- [16] A. N. Pfeiffer, C. Cirelli, A. S. Landsman, M. Smolarski, D. Dimitrovski, L. B. Madsen, and U. Keller, *Phys. Rev. Lett.* **109**, 083002 (2012).
- [17] D. Shafir, H. Soifer, B. Bruner, M. Dagan, Y. Mairesse, S. Patchkovskii, M. Ivanov, O. Smirnova, and N. Dudovich, *Nature (London)* **485**, 343 (2012).
- [18] C. Hofmann, A. S. Landsman, A. Zielinski, C. Cirelli, T. Zimmermann, A. Scrinzi, and U. Keller, *Phys. Rev. A* **90**, 043406 (2014).
- [19] B. Wolter, M. G. Pullen, M. Baudisch, M. Sclafani, M. Hemmer, A. Senftleben, C. D. Schröter, J. Ullrich, R. Moshhammer, and J. Biegert, *Phys. Rev. X* **5**, 021034 (2015).
- [20] O. Pedatzur, G. Orenstein, V. Serbinenko, H. Soifer, B. D. Bruner, A. J. Uzan, D. S. Brambila, A. G. Harvey, L. Torlina, F. Morales, O. Smirnova, and N. Dudovich, *Nat. Phys.* **11**, 815 (2015).
- [21] N. Camus, E. Yakaboylu, L. Fechner, M. Klaiber, M. Laux, Y. Mi, K. Z. Hatsagortsyan, T. Pfeifer, C. H. Keitel, and R. Moshhammer, *Phys. Rev. Lett.* **119**, 023201 (2017).
- [22] G. Porat, G. Alon, S. Rozen, O. Pedatzur, M. Krüger, D. Azoury, A. Natan, G. Orenstein, B. D. Bruner, M. J. J. Vrakking, and N. Dudovich, *Nat. Commun.* **9**, 2805 (2018).
- [23] U. S. Sainadh, H. Xu, X. Wang, A. Noor, W. Wallace, N. Douguet, A. Bray, I. Ivanov, K. Bartschat, A. Kheifets *et al.*, *Nature (London)* **568**, 75 (2019).
- [24] M. Li, H. Xie, W. Cao, S. Luo, J. Tan, Y. Feng, B. Du, W. Zhang, Y. Li, Q. Zhang, P. Lan, Y. Zhou, and P. Lu, *Phys. Rev. Lett.* **122**, 183202 (2019).
- [25] L. Torlina, F. Morales, J. Kaushal, I. Ivanov, A. Kheifets, A. Zielinski, A. Scrinzi, H. G. Muller, S. Sukiasyan, M. Ivanov, and O. Smirnova, *Nat. Phys.* **11**, 503 (2015).
- [26] M. Hentschel, R. Kienberger, C. Spielmann, G. A. Reider, N. Milosevic, T. Brabec, P. Corkum, U. Heinzmann, M. Drescher, and F. Krausz, *Nature (London)* **414**, 509 (2001).
- [27] A. Baltuška, T. Udem, M. Uiberacker, M. Hentschel, E. Goulielmakis, C. Gohle, R. Holzwarth, V. Yakovlev, A. Scrinzi, T. Hänsch *et al.*, *Nature (London)* **421**, 611 (2003).
- [28] G. Sansone, E. Benedetti, F. Calegari, C. Vozzi, L. Avaldi, R. Flammini, L. Poletto, P. Villoresi, C. Altucci, R. Velotta *et al.*, *Science* **314**, 443 (2006).
- [29] Q. Liu, L. Seiffert, A. Trabattoni, M. C. Castrovilli, M. Galli, P. Rupp, F. Frassetto, L. Poletto, M. Nisoli, E. Rühl *et al.*, *J. Opt.* **20**, 024002 (2018).
- [30] P. Ye, T. Csizmadia, L. Gulyás Oldal, H. N. Gopalakrishna, M. Füle, Z. Filus, B. Nagyillés, Zs. Divéki, T. Grósz, M. Dumergue *et al.*, *J. Phys. B: At., Mol. Opt. Phys.* **53**, 154004 (2020).
- [31] L. V. Keldysh, *Sov. Phys. JETP* **20**, 1307 (1965).
- [32] N. B. Delone and V. P. Krainov, *Phys.-Usp.* **41**, 469 (1998).
- [33] G. L. Yudin and M. Y. Ivanov, *Phys. Rev. A* **64**, 013409 (2001).
- [34] X. Wang, J. Tian, and J. H. Eberly, *Phys. Rev. Lett.* **110**, 243001 (2013).
- [35] N. Teeny, E. Yakaboylu, H. Bauke, and C. H. Keitel, *Phys. Rev. Lett.* **116**, 063003 (2016).
- [36] H. Ni, U. Saalmann, and J.-M. Rost, *Phys. Rev. Lett.* **117**, 023002 (2016).
- [37] J. Tian, X. Wang, and J. H. Eberly, *Phys. Rev. Lett.* **118**, 213201 (2017).
- [38] N. Douguet and K. Bartschat, *Phys. Rev. A* **97**, 013402 (2018).
- [39] M. Klaiber, K. Z. Hatsagortsyan, and C. H. Keitel, *Phys. Rev. Lett.* **120**, 013201 (2018).
- [40] R. Xu, T. Li, and X. Wang, *Phys. Rev. A* **98**, 053435 (2018).
- [41] S. Majorosi and A. Czirják, *Comput. Phys. Commun.* **208**, 9 (2016).
- [42] I. P. Christov, M. M. Murnane, and H. C. Kapteyn, *Phys. Rev. Lett.* **78**, 1251 (1997).
- [43] S. Majorosi, M. G. Benedict, and A. Czirják, *Phys. Rev. A* **98**, 023401 (2018).
- [44] W. P. Schleich, *Quantum Optics in Phase Space* (Wiley, New York, 2011).
- [45] A. Czirják, R. Kopold, W. Becker, M. Kleber, and W. Schleich, *Opt. Commun.* **179**, 29 (2000).
- [46] S. Gräfe, J. Doose, and J. Burgdörfer, *J. Phys. B: At., Mol. Opt. Phys.* **45**, 055002 (2012).
- [47] D. Heim, W. Schleich, P. Alsing, J. P. Dahl, and S. Varro, *Phys. Rev. Lett. A* **377**, 1822 (2013).
- [48] C. Baumann, H.-J. Kull, and G. M. Fraiman, *Phys. Rev. A* **92**, 063420 (2015).
- [49] H. Chomet, D. Sarkar, and C. F. de Morisson Faria, *New J. Phys.* **21**, 123004 (2019).
- [50] M. Han, P. Ge, Y. Fang, X. Yu, Z. Guo, X. Ma, Y. Deng, Q. Gong, and Y. Liu, *Phys. Rev. Lett.* **123**, 073201 (2019).
- [51] See Supplemental Material at <http://link.aps.org/supplemental/10.1103/PhysRevA.104.L031102> for an animation of the time dependent reduced 1D Wigner function of the hydrogen atom's electron driven by the laser pulse.
- [52] E. E. Serebryannikov and A. M. Zheltikov, *Phys. Rev. Lett.* **116**, 123901 (2016).
- [53] E. Madelung, *Z. Phys.* **40**, 322 (1927).